Letters

Modified Single-Loop Current Sensorless Control for Single-Phase Boost-Type SMR With Distorted Input Voltage

Hung-Chi Chen, *Member, IEEE*, Chih-Chieh Lin, and Jhen-Yu Liao

***Abstract*—The first single-loop current sensorless control (SLCSC) for single-phase boost-type switching-mode-rectifier (SMR) had been proposed in the prior paper. SLCSC with sinusoidal input voltage possesses good performance, but its performance with distorted input voltage should be improved. In this paper, a modified SLCSC is proposed and implemented in a field-programmable gate array (FPGA)-based system to obtain better performance than SLCSC. Instead of the phase-shift signal in SLCSC, the inductor voltage amplitude signal becomes the output of proportional-plus-integral (PI)-type voltage controller in the modified SLCSC. The provided simulation and experiment results demonstrate the modified SLCSC.**

***Index Terms*—Current sensorless control, switching mode rectifier.**

I. Introduction

A QUALIFIED ac/dc conversion includes functions of input current shaping and output voltage regulation. The use of switching-mode rectifier (SMR) is an effective mean to perform the qualified ac/dc conversion. Boost-type SMRs are the most popular circuit topology among all the others due to the continuous current in the inductor [1]. In order to save the input signals and pins, many current sensorless controls [2]–[5] had been proposed in this literature and are tabulated in Table I.

The current sensorless controls using the special function $d\,|\sin\theta|/d\theta$ are able to yield sinusoidal input current, even when the input voltage is distorted [2], [3]. On the other hand, those sensorless current controls with the assumption of sinusoidal input voltage have poor performance with distorted input voltage. In addition, the inductor resistance and the conducting voltages of switches and diodes are considered in [5], but are neglected in [2]–[4]. Sinusoidal input voltage is assumed in the proposed single-loop current sensorless control (SLCSC) [5], and significant increase of current harmonics can be found in the experimental results when the input voltage is distorted.

Manuscript received March 7, 2010; revised August 4, 2010; accepted August 17, 2010. Date of current version June 22, 2011. This work was supported by the National Science Council (NSC), Taiwan under Grant NSC98-2221-E-009-180-MY2. Recommended for publication by Associate Editor C. A. Canesin.

The authors are with the Department of Electrical Engineering, National Chiao Tung University (NCTU), Hsinchu 30010, Taiwan (e-mail: hcchen@cn.nctu.edu.tw; wahahi@gmail.com; popoid1003@hotmail.com).

Color versions of one or more of the figures in this paper are available online at http://ieeexplore.ieee.org.

Digital Object Identifier 10.1109/TPEL.2010.2070079

In this paper, the proposed SLCSC is modified to obtain good performance with distorted input voltage. Instead of the phase-shift signal in SLCSC, the inductor voltage amplitude signal becomes the output of the proportional-plus-integral (PI)-type voltage controller and the special function $d\,|\sin\theta|/d\theta$ is also used in the modified SLCSC.

First, the effects of inductor-voltage amplitude on the input current waveform are analyzed and modeled with considering the inductor resistance and conduction voltages. The result shows that the sinusoidal input current can be inherently yielded in modified SLCSC, even when the input voltage is distorted. Then, a PI-type voltage controller is included to regulate the output voltage by tuning this inductor voltage amplitude. Finally, some simulated and experimental results have been given to demonstrate the performance of the modified SLCSC.

II. Modified SLCSC

A. Boost-Type SMR

The boost-type SMR is plotted in Fig. 1, where it can be seen as a single-switch boost-type converter cascaded to a bridge rectifier. Resistors R_{s1}, R_{s2}, R_{o1}, and R_{o2} with resistances of several megaohms are used to sense the input voltage v_s and the output voltage V_o. In order to represent the resistance of the practical inductor, a resistor r_L is connected to an ideal inductor L in series.

In boost-type SMR, the input current $i_s(t)$ can be mathematically represented as

$$i_s(t) = \mathrm{sign}(v_s(t))i_L(t) \tag{1}$$

where $\mathrm{sign}(\cdot)$ is a sign operator and

$$\mathrm{sign}(X) = \begin{cases} +1, & \text{when } X \geq 0 \\ -1, & \text{when } X < 0. \end{cases} \tag{2}$$

During the positive input voltage, the input current i_s flows through D_3, r_L, L, T, and D_2, and through D_3, r_L, L, D, load, and D_2, when the switch T is turning on and turning off, respectively. Similarly, the current i_s flows through D_1, T, L, r_L, and D_4, and through D_1, load D, L, r_L, and D_4, when the switch T is conducting and blocking, respectively.

In order to develop the modified SLCSC, some assumptions are initially made.

1) The output voltage V_o is assumed to be equal to the voltage command V_o^* due to the bulk capacitor C_o.

TABLE I
SUMMARY OF CURRENT SENSORLESS CONTROL [2]–[5]

	[2]	[3]	[4]	[5]	Modified SLCSC
Assuming sinusoidal input voltage			√	√	
Special function $\frac{d\lvert\sin\theta\rvert}{d\theta}$ (i.e. $sign(\sin\theta)\cos\theta$)	√	√			√
Considering inductor resistance and conducting voltages of switches/diodes				√	√

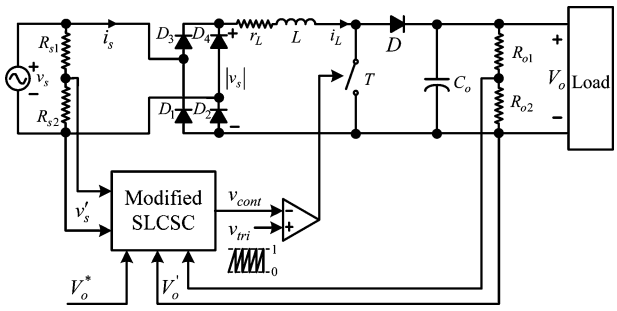

Fig. 1. Boost-type SMR with modified SLCSC.

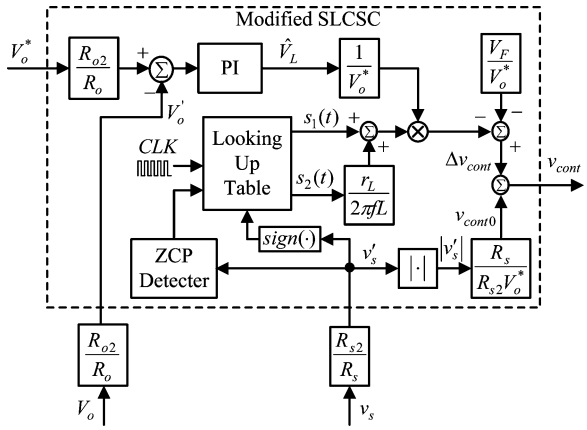

Fig. 2. Modified SLCSC.

2) The switching frequency $f_s(=1/T_s)$ is assumed to be much larger than the line frequency f and the input voltage is seen as constant during each switching period.
3) Both the sums of conduction voltages for the turning-ON loop and the turning-OFF loop are assumed to be equal to V_F.

The control signal $v_{\rm cont}$ in Fig. 1 is the output of the modified SLCSC and it is connected to the comparator $(-)$ terminal. A fixed-frequency fixed-amplitude carrier signal $v_{\rm tri}$ is at the comparator $(+)$ terminal. Based on the assumption 2), the average duty ratio $\bar{d}$ during each switching period T_s can be expressed as

$$\bar{d} = 1 - v_{\rm cont}. \tag{3}$$

Applying Kirchhoff's voltage law to the turning-ON loop and turning-OFF loop yields the turning-ON inductor voltage $v_{L,\rm ON}$ and turning-OFF inductor voltage $v_{L,\rm OFF}$, respectively

$$v_{L,\rm ON} = |v_s| - V_F - i_L r_L \tag{4}$$

$$v_{L,\rm OFF} = |v_s| - V_F - i_L r_L - V_o^*. \tag{5}$$

Then, the average inductor voltage $\bar{v}_L$ can be expressed as

$$\bar{v}_L = \frac{v_{L,\rm ON} \times t_{\rm ON} + v_{L,\rm OFF} \times t_{\rm OFF}}{T_s} \tag{6}$$

where $t_{\rm ON}(=\bar{d}T_s)$ and $t_{\rm OFF}(=T_s - t_{\rm ON})$ are the turning-ON time and turning-OFF time, respectively. By substituting (3), (4), and (5) into (6), the average inductor voltage can be rewritten as

$$\bar{v}_L = |v_s| - V_F - \bar{i}_L r_L - v_{\rm cont} V_o^*. \tag{7}$$

TABLE II
SIMULATED PARAMETERS

Input line voltage (rms)	$110Vrms$
Output voltage command	$V_o^* = 300V$
Input line frequency	$f = 60Hz$
Carrier frequency	$f_s = 50kHz$
Capacitance	$C_o = 470uF$
Sensing resistor	$R_{o1} = 910k\Omega$ $R_{o2} = R_{s2} = 10k\Omega$ $R_{s1} = 470k\Omega$
Inductance	$L = 4.56mH$
Inductor resistance	$r_L = 0.5\Omega$
Sum of conduction voltages	$V_F = 2.5V$
PI parameters	$K_P = 0.3V/V$ $K_I = 7500V/(V \cdot \sec)$

B. Modified SLCSC

According to the divider rule and the assumption of 1), the input signals v_s' and V_o' in Fig. 1 can be expressed as

$$v_s' = \frac{R_{s2}}{R_s} v_s \tag{8}$$

$$V_o' = \frac{R_{o2}}{R_o} V_o = \frac{R_{o2}}{R_o} V_o^* \tag{9}$$

where $R_s = R_{s1} + R_{s2}$ and $R_o = R_{o1} + R_{o2}$, respectively. By substituting (8) and (9) into (7), the average inductor voltage $\bar{v}_L$

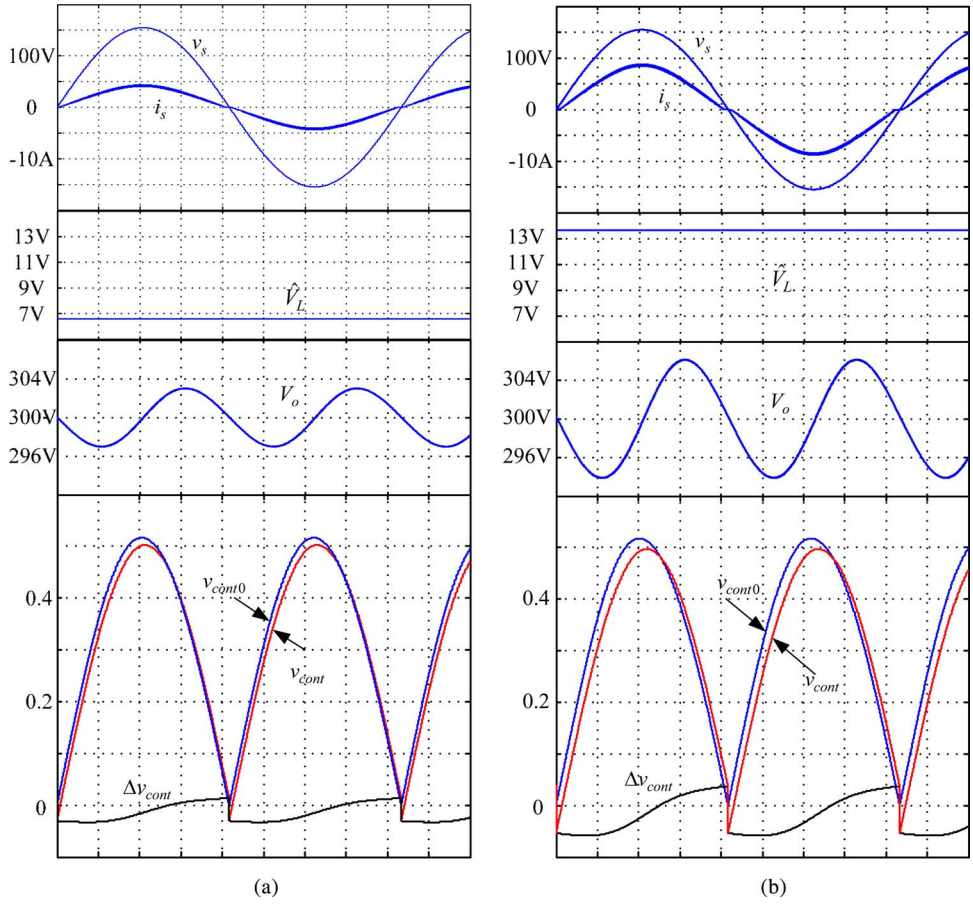

Fig. 3. Simulated waveforms for sinusoidal input voltage. (a) 300 W. (b) 600 W.

can be expressed as

$$\bar{v}_L = |v_s'| \frac{R_s}{R_{s2}} - V_F - \bar{i}_L r_L - v_{\rm cont} V_o' \frac{R_o}{R_{o2}}. \quad (10)$$

In order to yield the sinusoidal input current, the average inductor voltage $\bar{v}_L$ must be the function of $\text{sign}(v_s)\cos(2\pi ft)$ with amplitude $\hat{V}_L$, i.e.,

$$\bar{v}_L = \hat{V}_L \text{sign}(v_s)\cos(2\pi ft). \quad (11)$$

By substituting (11) into (10) and arranging the terms, the control signal $v_{\rm cont}$ is given as

$$v_{\rm cont} = v_{\rm cont0} + \Delta v_{\rm cont} \quad (12)$$

where the nominal control signal $v_{\rm cont0}$ and the variable control signal $\Delta v_{\rm cont}$ are

$$v_{\rm cont0} = |v_s'| \frac{R_s}{R_{s2}} \frac{1}{V_o^*} \quad (13)$$

$$\Delta v_{\rm cont} = \frac{\hat{V}_L}{V_o^*} \left[-s_1(t) - \frac{r_L}{2\pi f L} s_2(t) \right] - \frac{V_F}{V_o^*}. \quad (14)$$

It is noted that both unit functions $s_1(t) = \text{sign}(v_s')\cos(2\pi ft)$ and $s_2(t) = |\sin(2\pi ft)|$ are synchronized to the zero-crossing points (ZCPs) of the input voltage and repeated with fixed frequency (i.e., double line frequency $2f$). Thus, it is easy to generate functions $s_1(t)$ and $s_2(t)$ in a digital system.

TABLE III
SIMULATED THD_i VALUES

Average Output Power	Sinusoidal Input Voltage ($THD_v = 0$)	Distorted Input Voltage ($THD_v \approx 4.0\%$)
300W	5.63%	5.43%
400W	5.81%	5.43%
500W	6.05%	5.68%
600W	6.79%	6.01%

Fig. 2 shows the block diagrams of the modified SLCSC, where both functions $s_1(t)$ and $s_2(t)$ are generated by synchronizing the ZCPs of the input voltage signal v_s' and lookup table. In order to generate a signal with double line frequency $2f$, the frequency of the clock input *CLK* of the block "lookup table" is $f_s/(2f)$, where f_s is the sampling frequency (i.e., carrier frequency).

From the average inductor voltage in (11), the resulting average inductor current $\bar{i}_L$ and the average input current $\bar{i}_s$ can be

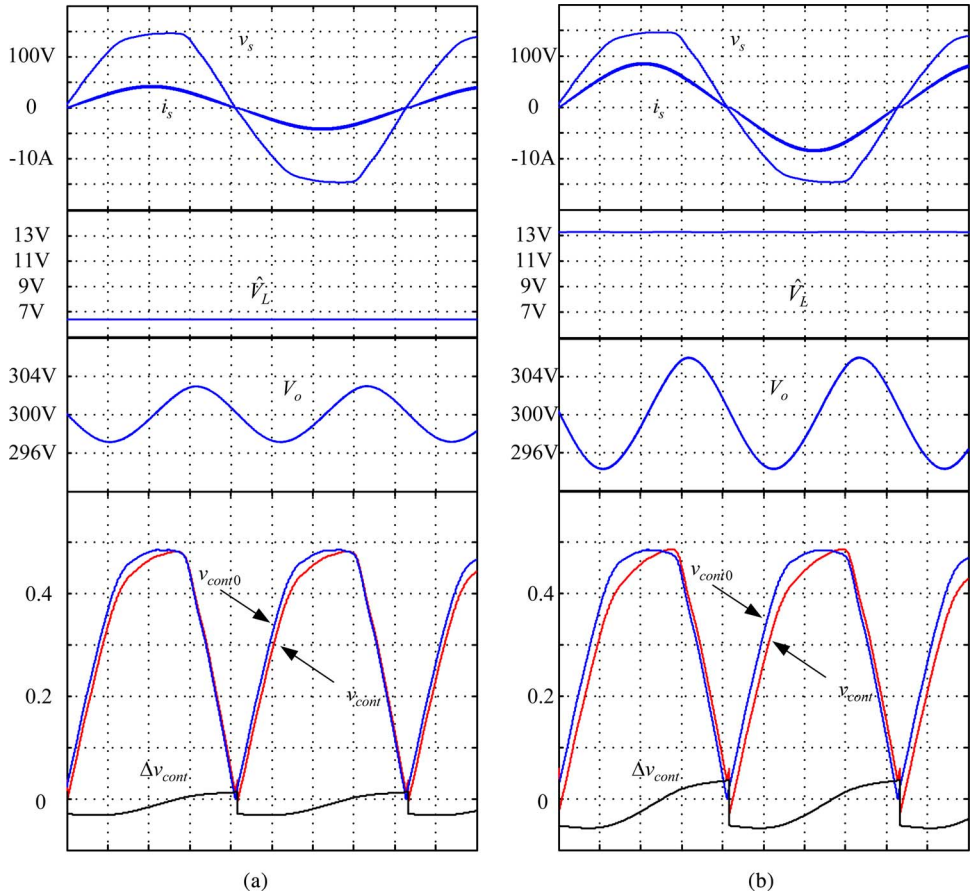

Fig. 4. Simulated waveforms for distorted input voltage. (a) 300 W. (b) 600 W.

expressed as

$$\bar{i}_L = \frac{\hat{V}_L}{2\pi f L} |\sin(2\pi f t)| \tag{15}$$

$$\bar{i}_s = \frac{\hat{V}_L}{2\pi f L} \sin(2\pi f t) = \hat{I}_s \sin(2\pi f t). \tag{16}$$

It is noted that the yielded input current i_s is sinusoidal and synchronized to ZCPs of the input voltage. In addition, the input current amplitude $\hat{I}_s$ is proportional to the inductor voltage amplitude $\hat{V}_L$, and thus, the average input power is also proportional to the inductor voltage amplitude $\hat{V}_L$.

In order to keep the output voltage constant, the average input power must be equal to the average load power. Therefore, based on the balance between the input power and output power, a PI-type controller is included in the modified SLCSC to regulate the output voltage by tuning the inductor voltage amplitude $\hat{V}_L$.

III. Simulation Results

In this section, some computer simulations in Physical Security Information Management (PSIM) software are performed to demonstrate the modified SLCSC. The simulated parameters are tabulated in Table II.

A. Sinusoidal Input Voltage

When the waveform of input voltage is sinusoidal, the simulated waveforms for average output power 300 and 600 W are plotted in Fig. 3(a) and (b), respectively. The normal control signal $v_{\rm cont0}$ is fixed regardless of the power level, but the variable control signal $\Delta v_{\rm cont}$ varies with the power level and the PI output $\hat{V}_L$.

The yielded input currents are sinusoidal and in phase with the sinusoidal input voltage, and the current amplitude are proportional to signal $\hat{V}_L$ in (16). Therefore, due to the balance between the input power and output power in simulation, the output voltages V_o are well regulated to 300 V.

The simulated total current harmonic distortion ($\rm THD_i$) values under various power levels are tabulated in Table III. In the simulation waveforms, the zero-crossing distortion increases with the power level, and thus, the simulated $\rm THD_i$ value also increases with the increase of power level.

B. Distorted Input Voltage

By replacing the sinusoidal input voltage with a distorted input voltage with total voltage harmonic distortion $\rm THD_v \approx 4.0\%$, the simulated waveforms for 300 and 600 W are plotted in Fig. 4(a) and (b), respectively, where the current waveforms in ZCP of input voltage are plotted in detail. The yielded input currents are sinusoidal and synchronizing to the distorted input

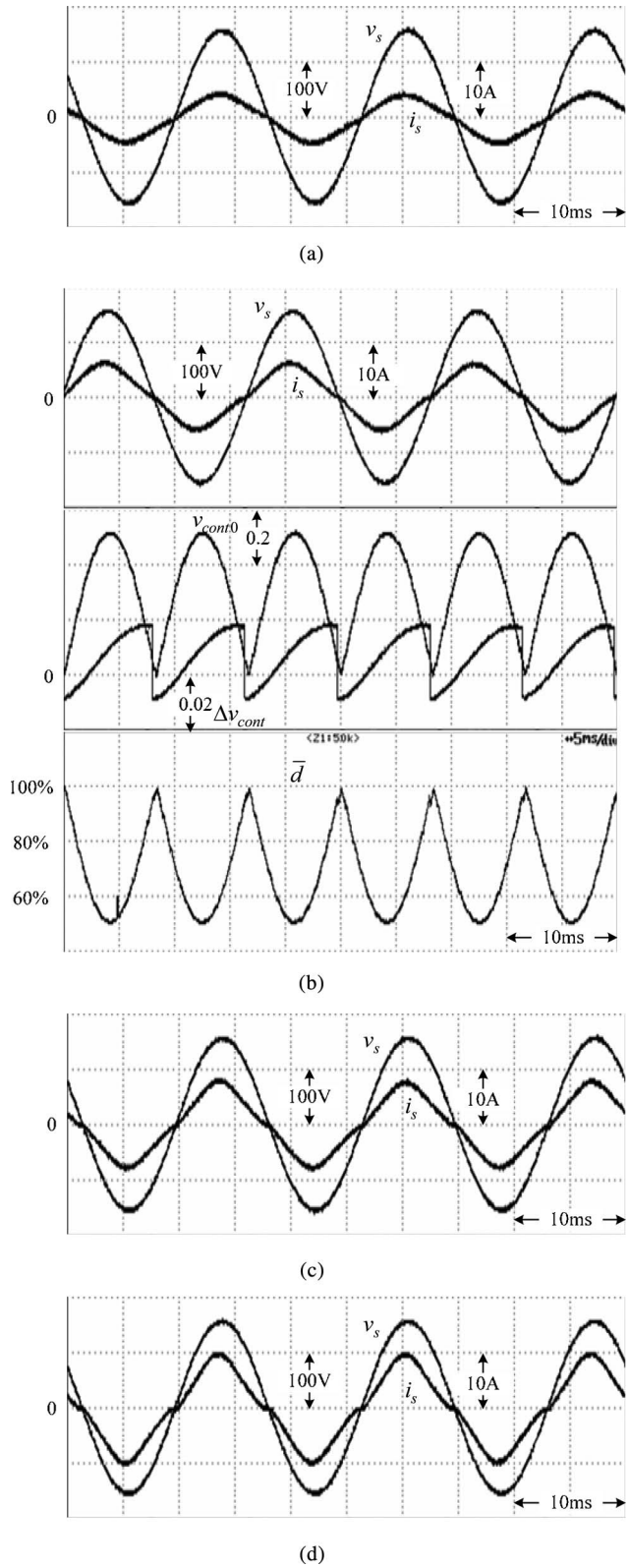

Fig. 5. Experimental results for sinusoidal input voltage for average output power. (a) 300 W. (b) 400 W. (c) 500 W. (d) 600 W.

voltage, and the current amplitude are proportional to the PI output $\hat{V}_L$ in (16). Due to the distorted input voltage, significant difference between the normal control signals $v_{\rm cont0}$ in Figs. 3 and 4 can be found.

TABLE IV
MEASURED THD_i VALUES

Average Output Power	Sinusoidal Input Voltage ($THD_v = 0$)	Distorted Input Voltage ($THD_v \approx 4.0\%$)
300W	7.56% (Fig. 5(a))	7.00% (Fig. 7(a))
400W	10.20% (Fig. 5(b))	7.34% (Fig. 7(b))
500W	12.08% (Fig. 5(c))	9.54% (Fig. 7(c))
600W	15.95% (Fig. 5(d))	12.23% (Fig. 7(d))

The simulated THD_i values of distorted input voltage according to various power levels are tabulated in Table III. Compared with Fig. 3, the waveforms of distorted input voltage in Fig. 4 show less zero-crossing distortion [6], and thus, the simulated THD_i values of distorted input voltage are lower than those of sinusoidal input voltage.

IV. EXPERIMENTAL RESULTS

In this section, some experimental results are provided to demonstrate the modified SLCSC, which had been digitally implemented in a field-programmable gate array (FPGA)-based system using Xilinx XC3S250E. The used parameters in the experiment are the same as those tabulated in Table I.

A. Sinusoidal Input Voltage

The sinusoidal input voltage is provided by the instrument of ac power source. Fig. 5 shows the experimental results for various output power where the average duty ratio $\bar{d}$, the control signals $v_{\rm cont0}$, and $\Delta v_{\rm cont}$ for 400 W are also plotted for comparison. When the input voltage is near zero, the average duty ratio is 100% in order to keep the switch conducting within several switching period. As the input voltage increases, the average duty ratio decreases. After the input voltage turns to decrease from its peak value, the average duty ratio increases from its minimum value.

Compared with the experimental results with sinusoidal input voltage in [5], the resulting input currents are more closed to the sinusoidal waveform in phase with the sinusoidal input voltage especially with low output power. Moreover, the current waveforms at low output power are significantly improved.

In the practical circuit, all the inductance, the equivalent inductor resistance, and the conduction voltages of diodes and switch are not constants and may vary with the instantaneous current. It means that parameter mismatches always exist in the system and have effects on the yielded current waveforms. However, the output voltage is well regulated by the PI-type controller from the experimental results.

Compared with the THD_i values from 14.3% (≈300 W) to 12.56% (≈600 W) in [5], the measured THD_i values tabulated in Table IV vary from 7.56% (300W) to 15.95% (600 W). Therefore, for experimental results with sinusoidal input voltage, the low-power performance is improved by the modified SLCSC.

In order to evaluate the transient performance of the modified SLCSC, the output power is suddenly increased from 300 to

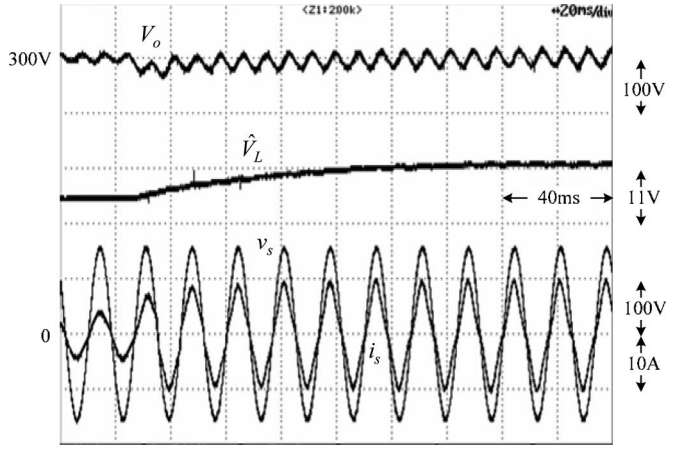

Fig. 6. Experimental waveforms for sinusoidal input voltage with the output power change from 300 to 600W.

600 W and the experimented waveforms are shown in Fig. 6. In order to regulate the output voltage to voltage command 300 V, the inductor voltage signal $\hat{V}_L$ increases and the resulting input current amplitude also increases. However, the input current is in phase with the sinusoidal input voltage during the transient time.

B. Distorted Input Voltage

In this experiment, the distorted input voltage, as shown in Fig. 7, is obtained by connecting the boost-type SMR to the electric outlet in the laboratory, where the measured total voltage harmonic distortion is $\mathrm{THD}_v \approx 4.0\%$.

Fig. 7(a)–(d) shows the experimental results for output power 300, 400, 500, and 600 W, respectively, where the average duty ratio $\bar{d}$, the control signals $v_{\mathrm{cont}0}$, and Δv_{cont} for 400 W are also plotted for comparison.

Compared with the measured THD_i values from 20.4% (≈300W) to 12.0% (≈700 W) in [5], the measured THD_i values tabulated in Table IV vary from 7.00% (300 W) to 12.23% (600 W). Therefore, from the experimental results of distorted input voltage, the low-power performance is significantly improved by the modified SLCSC.

The current harmonics of the current waveforms in Figs. 5 and 7 are tabulated in Table V, where the harmonic limits of the IEC-61000-3-2 for Class A and Class D are also listed for comparison. The yielded current harmonics are well below the harmonic limits, and thus, the measured currents comply with the commercial standards.

It is noted that the yield input current is synchronized with the ZCPs, not in phase with the fundamental component of the distorted input voltage. Thus, the measured fundamental input currents of distorted input voltage are slightly larger than those of sinusoidal input voltage due to the displacement power factor.

From the simulation results in Table III and the experimental results in Table IV, all the measured THD_i values of distorted input voltage are smaller than those of sinusoidal input voltage. It follows that the modified SLCSC with distorted input voltage has better performance than with sinusoidal input voltage.

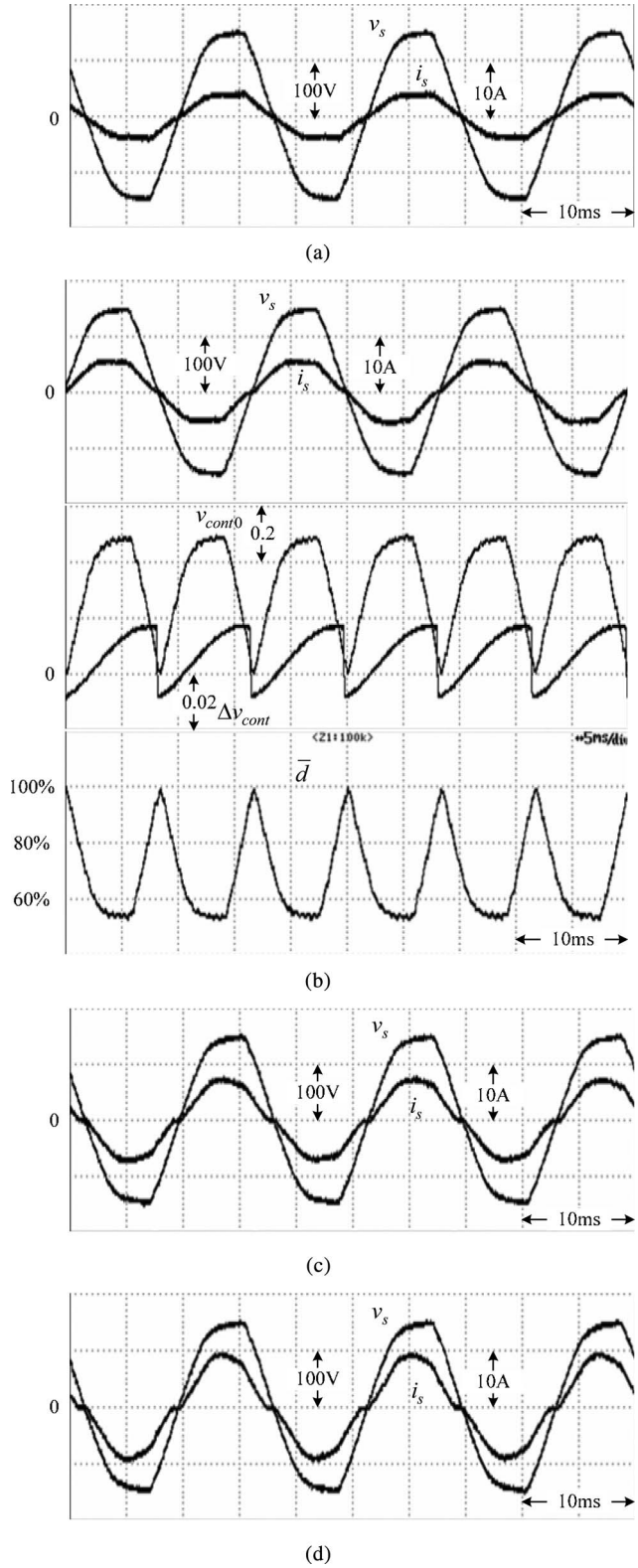

Fig. 7. Experimental results for distorted input voltage for average output power. (a) 300 W. (b) 400 W. (c) 500 W. (d) 600 W.

In order to evaluate the transient performance with distorted input voltage, the load power is forced to have a step change from 300 to 600 W and the experimented waveforms are shown in Fig. 8. In order to keep the output voltage to voltage command

TABLE V
MEASURED CURRENT HARMONICS

Order	Class A (A_{rms})	300W Class D (A_{rms})	300W Fig.5(a) (A_{rms})	300W Fig.7(a) (A_{rms})	600W Class D (A_{rms})	600W Fig.5(d) (A_{rms})	600W Fig.7(d) (A_{rms})
Fund.	**X**	**X**	2.8992	2.9147	**X**	5.9563	6.0693
3	**2.3**	**1.02**	0.2057	0.1078	**2.04**	0.9201	0.5962
5	**1.14**	**0.57**	0.0337	0.1716	**1.14**	0.0581	0.3597
7	**0.77**	**0.3**	0.0161	0.0555	**0.6**	0.1159	0.1456
9	**0.4**	**0.15**	0.0110	0.0217	**0.3**	0.0712	0.0537
11	**0.33**	**0.105**	0.0099	0.0318	**0.21**	0.0530	0.0788
13	**0.21**	**0.089**	0.0067	0.0225	**0.178**	0.0343	0.0513
15	**0.15**	**0.077**	0.0036	0.0106	**0.154**	0.0209	0.0136
17	**0.132**	**0.068**	0.0038	0.0104	**0.136**	0.0155	0.0077
19	**0.118**	**0.061**	0.0029	0.0097	**0.122**	0.009	0.0112

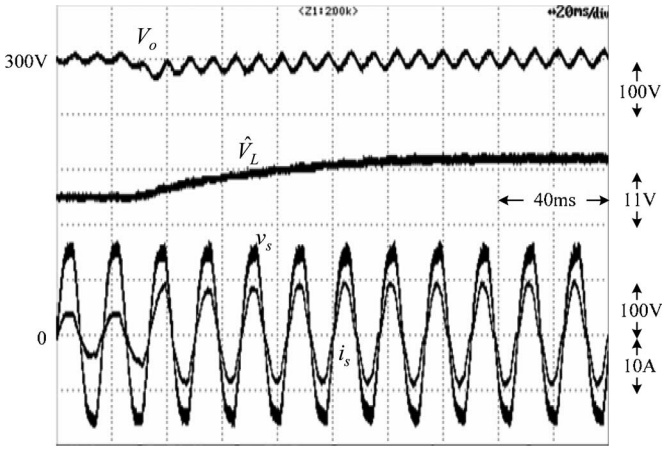

Fig. 8. Experimental waveforms for the distorted input voltage when the load is suddenly changed from 300 to 600W.

300 V, the output $\hat{V}_L$ of the PI controller increases and the resulting input current amplitude also increases to meet the requirement of power balance. However, the input current can be seen as being synchronized with the sinusoidal input voltage during the transient period.

V. CONCLUSION

The modified SLCSC has been proposed and implemented in this paper and it yields lower current harmonics than the prior SLCSC. In addition, the modified SLCSC with distorted input voltage possesses better performance than that with sinusoidal input voltage. However, due to the parameter mismatch, the practical input current is near sinusoidal, and fortunately, the current harmonics are lower than the well-known harmonic limits.

REFERENCES

[1] O. Garcia, J. A. Cobos, R. Prieto, P. Alou, and J. Uceda, "Single phase power factor correction: A survey," *IEEE Trans. Power Electron.*, vol. 18, no. 3, pp. 749–754, May 2003.

[2] T. Ohnishi and M. Hojo, "DC voltage sensorless single-phase PFC converter," *IEEE Trans. Power Electron.*, vol. 19, no. 2, pp. 404–410, Mar. 2004.

[3] S. Sivakumar, K. Natarajan, and R. Gudelewicz, "Control of power factor correcting boost converter without instantaneous measurement of input current," *IEEE Trans. Power Electron.*, vol. 10, no. 4, pp. 435–445, Jul. 1995.

[4] Y. K. Lo, H. J. Chiu, and S. Y. Ou, "Constant-switching-frequency control of switch mode rectifiers without current sensors," *IEEE Trans. Ind. Electron.*, vol. 47, no. 5, pp. 1172–1174, Oct. 2000.

[5] H. C. Chen, "Single-loop current sensorless control for single-phase boost-type SMR," *IEEE Trans. Power Electron.*, vol. 24, no. 1, pp. 163–171, Jan. 2009.

[6] J. Sun, "On the zero-crossing distortion in single-phase PFC converters," *IEEE Trans. Power Electron.*, vol. 19, no. 3, pp. 685–692, Mar. 2004.